Buoyancy-induced recirculation bubbles and heat convection of developing flow in vertical channels with fin arrays

Chin-Hsiang Cheng and Jyh-Jye Yang
Department of Mechanical Engineering, Tatung Institute of Technology, Taipei, Taiwan, R.O.C.

Developing fluid flow and heat transfer characteristics of the mixed convection in a vertical parallel-plate channel with fin array are analyzed in this study. The channel walls are maintained at uniform but unequal temperatures, and the fins of extremely high thermal conductivity are mounted on the relatively hotter wall. The stream function-vorticity method coupled with the power-law scheme are employed to solve the continuity, momentum and energy equations numerically. Results show that the streamwise periodic variation of the cross-sectional area causes the flow and temperature fields to attain a periodically fully developed character after a number of modules from the inlet. Meanwhile, if wall heating is sufficiently strong, an adverse pressure gradient can be developed downstream in the channel, and a series of buoyancy-induced recirculation bubbles may appear adjacent to the colder wall. The periodically fully developed solutions provided by Cheng et al. (*Int. J. Heat Mass Transfer* 1992, **35**, 2643–2653) are found to accurately portray the behavior of the present developing flow in the downstream region.

Keywords: recirculation bubbles; mixed convection; vertical channel; fin array

Introduction

Convective heat transfer of laminar duct flow has been an interesting topic to researchers in the last several decades, since it is frequently encountered in heat transfer or fluid devices. A comprehensive survey of the literature pertinent to heat transfer behavior and friction loss in the entrance and fully developed regions has been provided by Shah and London (1978).

Since the overall heat transfer coefficients of laminar flow in the smooth channels are insufficient for real applications, the augmentation of heat transfer becomes particularly important. In augmentation techniques, fins of high thermal conductivity are usually attached to the channel walls so as to protrude into the convective flow field to enhance heat transfer. These fins provide additional surface area for heat transfer and improve the mixing of the flow so as to increase the heat transfer coefficients on the walls. One may see the application of fins in many thermal systems, such as solar collectors, nuclear reactors, heat exchangers, and electronic equipment.

For the channel with only one or two fins, Durst et al. (1988) and Cheng and Huang (1989) studied the flow separation and reattachment behavior for various geometric arrangements and Reynolds numbers. The effect of the transverse fins placed in entrance regions on heat transfer and friction loss of the developing flow was also evaluated.

When the number of fins in the channel is increased, a streamwise-periodic flow pattern may develop after sufficient distance for development. That is, considering one module region between two successive fins, the outflow profiles will become nearly the same as the inflow profiles. This pattern was observed experimentally by Berner et al. (1984). For analyzing this periodically fully developed flow, a theoretical method was provided by Patankar et al. (1977). And based on the concepts described by Patankar et al. (1977), many authors, such as Webb and Ramadhyani (1985), Kelkar and Patankar (1987), Cheng and Huang (1991), and Luy et al. (1991), have further investigated this periodic character of pure forced-convection flow in finned channels.

However, it is recognized that the validity of the above-cited forced-convection analyses is restricted to cases with very high flow velocity or slight wall heating, in which the effect of buoyancy force is negligible. In many cases of interest, the buoyancy force arising from the temperature difference may play an important role in heat transfer. Consequently, the assumption of negligible buoyancy in theoretical model can cause significant error. Therefore, in recent years, the problems of combined free and forced convection of duct flow have received considerable attention. In fact, increasing attention has been focused on a buoyancy-induced flow-reversal phenomenon in unfinned smooth channels. Considering smooth vertical channels with unequal wall temperatures, Aung and Wouku (1986a, 1986b) presented the numerical solution of developing flow and the analytical solution of fully developed flow as well. They found that when the wall heating is sufficiently intense, flow reversal can occur near the relatively colder wall in a buoyancy-assisting situation. Recently, Cheng et al. (1990) extended and solved the fully developed problems by considering more thermal boundary conditions, and the parameter zones for the occurrence of reversed flow under various boundary conditions were found.

Being aware that buoyancy has a profound influence on flow pattern and thermal characteristics in unfinned channels (Aung and Worku 1986a, 1986b; Cheng et al. 1990), one may expect

Address reprint requests to Professor Cheng at the Department of Mechanical Engineering, 40 Chungshan North Road Sec. 3, Taipei, Taiwan, R.O.C.

Received 1 December 1992; accepted 2 September 1993

that in a finned channel, the influence of buoyancy is likewise appreciable and worthy of investigation. Cheng et al. (1992) have evaluated the buoyancy effect on the periodic character of the fully-developed flow in vertical channels with fin array. They found that in addition to the typical "primary" recirculation vortex behind each fin, a buoyancy-driven "secondary" vortex bubble appears adjacent to the colder wall within one module as the Grashof number is greater than a critical value. The strength and size of this secondary vortex bubble can be altered by changing the geometric parameters.

The analysis of Cheng et al. (1992) was focused on the periodically fully developed region that could only be found downstream. However, for real devices, the flow field in channels includes not only the fully developed region but also the entrance zone. When the overall length of channel is limited, the developing flow in the entrance zone becomes particularly important, and hence, needs to be taken into consideration. Under these circumstances, the present study performs numerical analysis to evaluate the influence of buoyancy force on the developing flow in the entrance region, in order to extend the investigation of Cheng et al. (1992) and to explore the development process of the downstream periodic flow.

Figure 1 shows the physical model of a vertical parallel-plate channel with fin array. The fins of the same height (e) are placed at equal streamwise space (d). Fin thickness is assumed to be negligible in comparison with the pitch length. Wall 1 ($y = 0$) is the heating wall, which is maintained at a higher temperature (T_1), and wall 2 ($y = H$) is at the ambient temperature without heating (T_0).

The thermal conductivity of fin material is considered to be very high so that the temperature of fin surface is uniform and equal to the attached wall temperature. Theoretically speaking, the thermal boundary conditions on the fin surfaces are dependent mainly on the conduction of the fin material. As discussed by Sparrow et al. (1978), if the fins are sufficiently thin, the temperature variation within fin thickness can be ignored. Then the temperature variation along the fin will be governed by a fin-conductance parameter C, given by $C = k_{fin}t/(kd)$. Such a parameter has been used by Sparrow et al. (1978), and its influence has also been evaluated by Kelkar and Patankar (1987) and Lazaridis (1988). For a very large value of C, the temperature of the fin surface is uniform and equal to the attached wall temperature. Based on the studies of Kelkar and Patankar (1987) and Lazaridis (1988), the relative error in heat transfer rate between the cases $C = 100$ and $C = \infty$ is within 2 percent. This implies that the uniform fin-temperature assumption produces a rather small error as C greater than 100. Note that, for example, the conductivity ratio k_{fin}/k for a copper–air system can reach 1.5×10^4. In this case, even if the value of t/d is scaled to 0.007 (a negligible thickness), the value of C is still greater than 100. Thus, the assumption of uniform fin surface temperature made in this study is reasonable and retains sufficient value in practical application.

The ambient fluid at T_0 enters the channel with a uniform velocity profile and goes upwards. The velocity and temperature profiles at successive streamwise locations separated by one pitch will gradually exhibit the periodic character after a number of modules from the inlet.

Basically, flow behavior is governed by the Reynolds number, Grashof number, and the geometric parameters such as fin height (e/H) and fin pitch (d/H). Since the effect of buoyancy force becomes particularly appreciable in the low Reynolds number cases, only the results of $Re \leq 300$ are presented. The Grashof number is up to 10^5, and the ranges of fin pitch and fin height are considered to be within $1 \leq d/H \leq 4$ and $0 \leq e/H \leq 0.5$, respectively. Besides, the Prandtl number of fluid is also an important factor to the flow and thermal fields. A higher Prandtl number always produces higher heat transfer rates, as already discussed by Patankar et al. (1977), Webb and Ramadhyani (1985), Kelkar and Patankar (1987), and Cheng and Huang (1991). In this study, the value of the Prandtl number is fixed at 0.71 for air flow, without consideration of the Prandtl number effect.

It is important to mention that when the fin height

Notation

C	Fin conductance parameter
D	Dimensionless pitch length of fin array
d	Pitch length of fin array
D_h	Hydraulic diameter
E	Dimensionless fin height
e	Fin height
Gr	Grashof number
g	Gravitational acceleration
H	Channel width
k	Thermal conductivity of fluid
k_{fin}	Thermal conductivity of fin material
L	Length of entire solution domain
P	Dimensionless fluid pressure
Pr	Prandtl number
p^*	Hydrostatic pressure
p	Fluid pressure
Q	Dimensionless overall heat transfer in one module length
Q_f	Dimensionless overall heat transfer on fin surface
Q_0	Dimensionless overall heat transfer in one module length for forced-convection flow in a smooth channel
Q_1 Q_2	Dimensionless overall heat transfer on walls 1 and 2 in one module
Q_{1x}, Q_{2x}	Dimensionless local heat fluxes on walls 1 and 2
Re	Reynolds number
S_{min}	Minimum dimensionless stream function in one module
T	Fluid temperature
t	Fin thickness
U	Dimensionless fluid velocity in x-direction
u	Fluid velocity in x-direction
V	Dimensionless fluid velocity in y-direction
v	Fluid velocity in y-direction
X, Y	Dimensionless coordinate system
x, y	Rectangular coordinate system
x_{FD}	Entrance length

Greek symbols

α	Thermal diffusivity of fluid
β	Coefficient of volumetric expansion of fluid
θ	Dimensionless fluid temperature
ν	Kinematic viscosity of fluid
ρ	Fluid density
Ψ	Dimensionless stream function
ψ	Stream function
Ω	Dimensionless fluid vorticity
ω	Fluid vorticity

Subscripts

0	Smooth channel/inlet condition/colder wall
1	Hotter wall 1
2	Colder wall 2

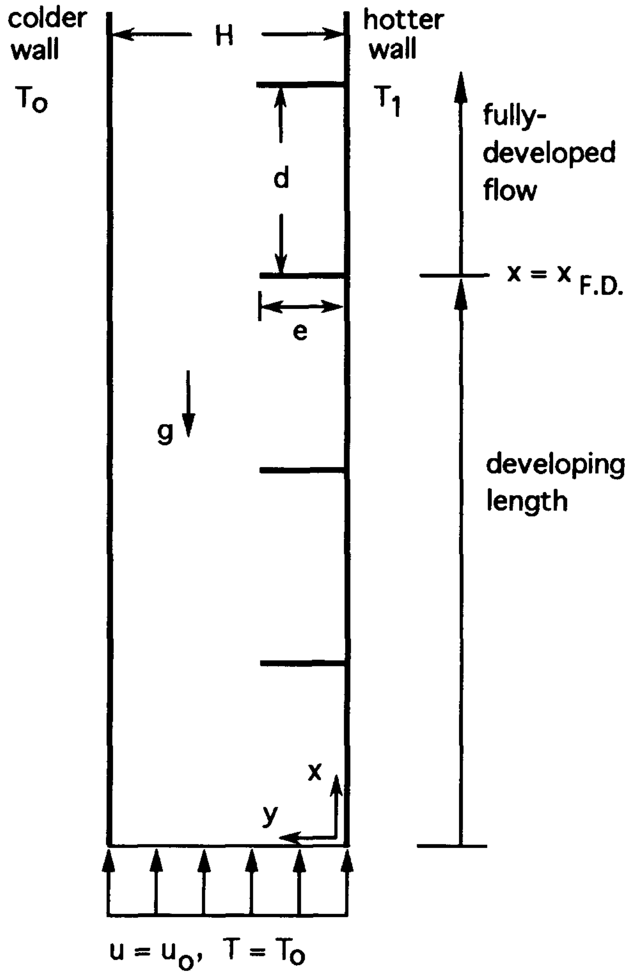

Figure 1 A vertical channel with fin array

approaches zero, the present numerical solutions should approach to the solutions presented by Cheng et al. (1990) and Aung and Worku (1986a, 1986b) for the smooth channels. Meanwhile, the solutions at far downstream location should be verified by the periodically fully developed solutions provided by Cheng et al. (1992) and Luy et al. (1991). The excellent agreement between the present numerical results and those of the earlier studies will be seen later.

Theoretical analysis

Governing equations

The flow and temperature fields are assumed to be two-dimensional (2-D) and laminar with constant properties, except for the variation of density in the buoyancy term of the momentum equation. The computation procedures have been described in detail in earlier studies (Cheng and Huang 1989, 1991; Luy et al. 1991; Cheng et al. 1992); therefore, the statements in the following sections will be limited to the main features of the mathematical formulation and the treatment in downstream boundary conditions.

Stream function–vorticity method is used herein to obtain the velocity solutions. Without the awkwardness in handling the pressure term, this method inherently exhibits better efficiency by saving computation time for 2-D flow analysis. The stream function and vorticity are defined by

$$u = \frac{\partial \psi}{\partial y} \tag{1}$$

$$v = -\frac{\partial \psi}{\partial x} \tag{2}$$

and

$$\omega = \frac{\partial v}{\partial x} - \frac{\partial u}{\partial y} \tag{3}$$

respectively.

The dimensionless governing equations of the 2-D, steady, incompressible, constant-property flow in the developing region of a vertical finned channel are expressed in the stream function-vorticity formulation as

$$\frac{\partial^2 \Psi}{\partial X^2} + \frac{\partial^2 \Psi}{\partial Y^2} = -\Omega \tag{4}$$

$$\frac{\partial \Psi}{\partial Y}\left(\frac{\partial \Omega}{\partial X}\right) - \frac{\partial \Psi}{\partial X}\left(\frac{\partial \Omega}{\partial Y}\right) = \frac{2}{\mathrm{Re}}\left(\frac{\partial^2 \Omega}{\partial X^2} + \frac{\partial^2 \Omega}{\partial Y^2}\right) - \frac{\mathrm{Gr}}{2\,\mathrm{Re}^2}\frac{\partial \theta}{\partial Y} \tag{5}$$

$$\frac{\partial \Psi}{\partial Y}\left(\frac{\partial \theta}{\partial X}\right) - \frac{\partial \Psi}{\partial X}\left(\frac{\partial \theta}{\partial Y}\right) = \frac{2}{\mathrm{Pr}\,\mathrm{Re}}\left(\frac{\partial^2 \theta}{\partial X^2} + \frac{\partial^2 \theta}{\partial Y^2}\right) \tag{6}$$

with the following dimensionless parameters:

$$X = \frac{x}{H}, \quad Y = \frac{y}{H}, \quad \theta = \frac{T - T_0}{T_1 - T_0}, \quad \Psi = \frac{\psi}{u_0 H}, \quad \Omega = \frac{\omega H}{u_0}, \quad \mathrm{Pr} = \frac{\nu}{\alpha} \tag{7}$$

Indicating the strength of buoyancy force, the Grashof number (Gr) is given by

$$\mathrm{Gr} = \frac{g\beta(T_1 - T_0)D_h^3}{\nu^2} \tag{8}$$

$\mathrm{Gr} = 0$ represents the pure forced-convection situation. Meanwhile, the Reynolds number is defined by

$$\mathrm{Re} = \frac{u_0 D_h}{\nu} \tag{9}$$

In the above equations, the hydraulic diameter (D_h) is twice the channel width for a parallel-plate channel, and u_0 is referred to as the inlet velocity of fluid flow.

Boundary conditions

The fluid enters the channel with a uniform velocity and at ambient temperature, which can be directly prescribed before calculation. That is, in terms of stream function and vorticity, the boundary conditions at the inlet may be expressed as

$$\Psi = Y,\ \Omega = -\frac{\partial^2 \Psi}{\partial X^2},\ \frac{\partial \Psi}{\partial X} = 0, \text{ and } \theta = 0, \text{ at } X = 0 \tag{10a}$$

The conditions on the channel wall surfaces are

$$\Psi = 0,\ \Omega = -\frac{\partial^2 \Psi}{\partial Y^2},\ \frac{\partial \Psi}{\partial Y} = 0, \text{ and } \theta = 1, \text{ at } Y = 0 \tag{10b}$$

$$\Psi = 1,\ \Omega = -\frac{\partial^2 \Psi}{\partial Y^2},\ \frac{\partial \Psi}{\partial Y} = 0, \text{ and } \theta = 0, \text{ at } Y = 1 \tag{10c}$$

The boundary conditions on the fin surfaces are

$$\Psi = 0,\ \Omega = -\frac{\partial^2\Psi}{\partial X^2},\ \frac{\partial\Psi}{\partial X} = 0,\ \text{and}\ \theta = 1 \tag{10d}$$

However, at the downstream face of the last module, the conditions of velocity and temperature are basically unknown. One needs to assign the periodic flow character to the upstream and downstream faces of the last module and carry out the profiles of velocity and temperature downstream with an iterative process. The periodic character of stream function, vorticity, and temperature downstream can be given as

$$\Psi(L, Y) = \Psi(L - d/H, Y) \tag{11a}$$

$$\Omega(L, Y) = \Omega(L - d/H, Y) \tag{11b}$$

$$\theta(L, Y) = \theta(L - d/H, Y) \tag{11c}$$

where $X = L$ and $X = L - d/H$ represent the downstream and upstream faces of the last module, respectively, and L is the entire dimensionless channel length of interest.

Dimensionless heat transfer and pressure variation

Once the velocity and temperature fields are carried out, the local heat transfer can be further calculated. The dimensionless local heat fluxes on the respective walls are defined as

$$Q_{1x} = -\frac{H}{T_1 - T_0}\frac{\partial T}{\partial y}\bigg|_{y=0} = -\frac{\partial\theta}{\partial Y}\bigg|_{Y=0} \tag{12a}$$

and

$$Q_{2x} = -\frac{H}{T_1 - T_0}\frac{\partial T}{\partial y}\bigg|_{y=H} = -\frac{\partial\theta}{\partial Y}\bigg|_{Y=1} \tag{12b}$$

And the dimensionless heat flux on fin surfaces is given by

$$Q_{fy} = \pm\frac{H}{T_1 - T_0}\frac{\partial T}{\partial x}\bigg|_{\text{fin}} = \pm\frac{\partial\theta}{\partial X}\bigg|_{\text{fin}} \tag{12c}$$

where the sign "$\pm$" is chosen to make positive values of Q_{fy} for different sides of the fin.

Overall heat transfer from walls (Q_1, Q_2) within one module can be evaluated by the integration of local heat flux (Q_{1x}, Q_{2x}) with respect to X in one pitch length.

On the other hand, the axial variation of the dimensionless pressure

$$P = \frac{p - p_0}{\rho u_0^2} \tag{13}$$

can be calculated by integrating the dimensionless momentum equation in x-direction

$$\frac{\partial P}{\partial X} = \frac{2}{\text{Re}}\left(\frac{\partial^3\Psi}{\partial X^2\,\partial Y} + \frac{\partial^3\Psi}{\partial Y^3}\right) + \frac{\text{Gr}}{2\,\text{Re}^2}\theta - \left[\frac{\partial\Psi}{\partial Y}\left(\frac{\partial^2\Psi}{\partial X\,\partial Y}\right) - \frac{\partial\Psi}{\partial X}\left(\frac{\partial^2\Psi}{\partial Y^2}\right)\right] \tag{14}$$

In the present study, the pressure at $Y = Y_0 = 0.5(1 + e/H)$, the midpoint of the free-passing space of each cross section, is calculated to show the axial pressure variation. Furthermore, the difference between the pressures at the downstream and upstream faces of each module can be used to calculate the overall pressure gradient within each module (dP/dX) as

$$\frac{dP}{dX} = [P(X + d/H, Y_0) - P(X, Y_0)]/(d/H) \tag{15}$$

Grid system

Through a procedure of carefully checking the grid independence of the numerical solutions, a grid system of 1601×41 (in $x \times y$ directions) grid points in the entire solution domain is adopted typically in the computation. Part of the results of the grid-independent check will be displayed in the next section. Meanwhile, to ensure that the numerical solutions of developing flow is independent of the number of fins covered in the solution domain, four numbers, 20, 30, 40, and 50, are tested individually. In consequence, it is found that 40 fins is sufficiently long for the flow to become fully developed in the range of parameters considered here. The entire solution domain consists of 40 fins so that there are 41×41 grid points placed within each module. Meanwhile, the entire channel length could be 40 to 160 times the channel width when the dimensionless pitch length (d/H) is varied from 1 to 4.

Results and discussion

Data check with benchmark solutions

The present numerical solution of velocity at far downstream location in a smooth channel ($e/H = 0$) is first compared with the analytical fully developed solution for mixed convection flow presented by Aung et al. (1986b). Figure 2a demonstrates the excellent agreement in data comparison for velocity profiles under various values of Gr/Re. Note that the reversed flow adjacent to the colder wall appears if Gr/Re exceeds a critical value. The curve of Gr/Re = 0 indicates the pure forced-convection flow, which is just the Poiseuille parabolic profile. Besides, the developing velocity profiles for forced-convection flow at Re = 40, shown in Figure 2b, are also checked with the results of Morihara and Cheng (1973). It is found that the numerical solution basically matches the results of these previous studies.

In addition, some existing data of the entrance length in a smooth channel ($e/H = 0$) for pure forced-convection flow (Gr/Re = 0) are also adopted to check the present obtained results. Table 1 displays the dimensionless length of the developing region (x_{FD}/H) as a function of the Reynolds number, comparing the present results with some existing data (Morihara and Cheng 1973; Brandt and Gillis 1966; Chen 1973; Narang and Krishnamoorthy 1976). The definition of entrance length is based on the same criterion proposed in these existing papers.

Flow and temperature fields

Results of the flow pattern and thermal field under various physical parameters are provided in this section. Although typically 40 modules are considered in the entire solution domain, the region of the first 10 modules is in general enough to display the developing flow.

Figure 3 shows the influence of fin height on the developing flow for Re = 100, $d/H = 2$, and Gr = 10^5. In the case of $e/H = 0$, flow separation occurs adjacent to the colder wall after a certain distance from the inlet. The reversed flow pattern starts to develop and then becomes fully developed downstream. The location of the separation point moves to the inlet if Gr is increased. It is interesting to find that the reversed flow pattern is significantly altered by the existence of a fin array. When a fin array exists but e/H is small (say 0.1), a small vortex behind each fin can be seen, whereas the main feature of the reversed flow near the colder wall is only slightly changed. However, as the fin height is elevated, the reversed flow zone is apparently "suppressed" into a series of separate

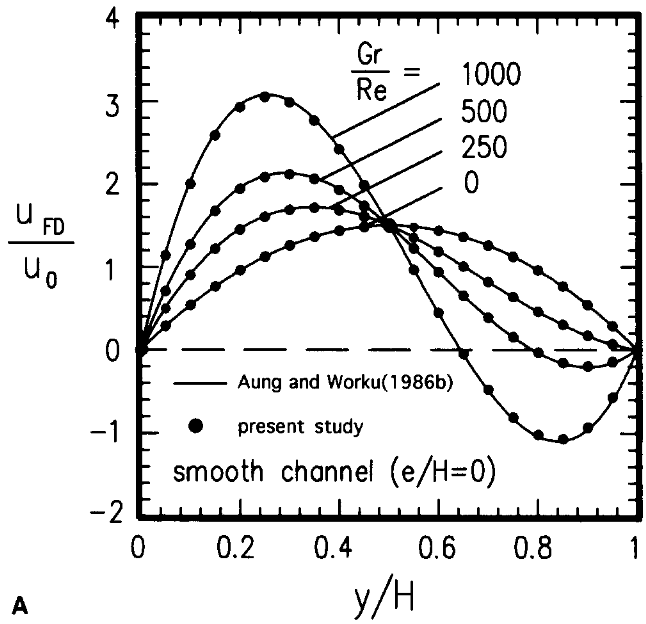

A

Re = 40

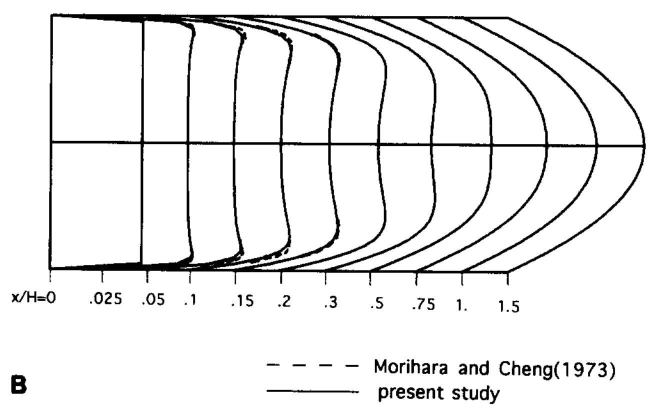

B

Figure 2 Data check with benchmark solutions of smooth-channel flows. (a) Fully developed velocity profiles of mixed-convection flow, compared with Aung and Worku (1986b); (b) developing velocity profiles of pure forced-convection flow, compared with Morihara and Cheng (1973)

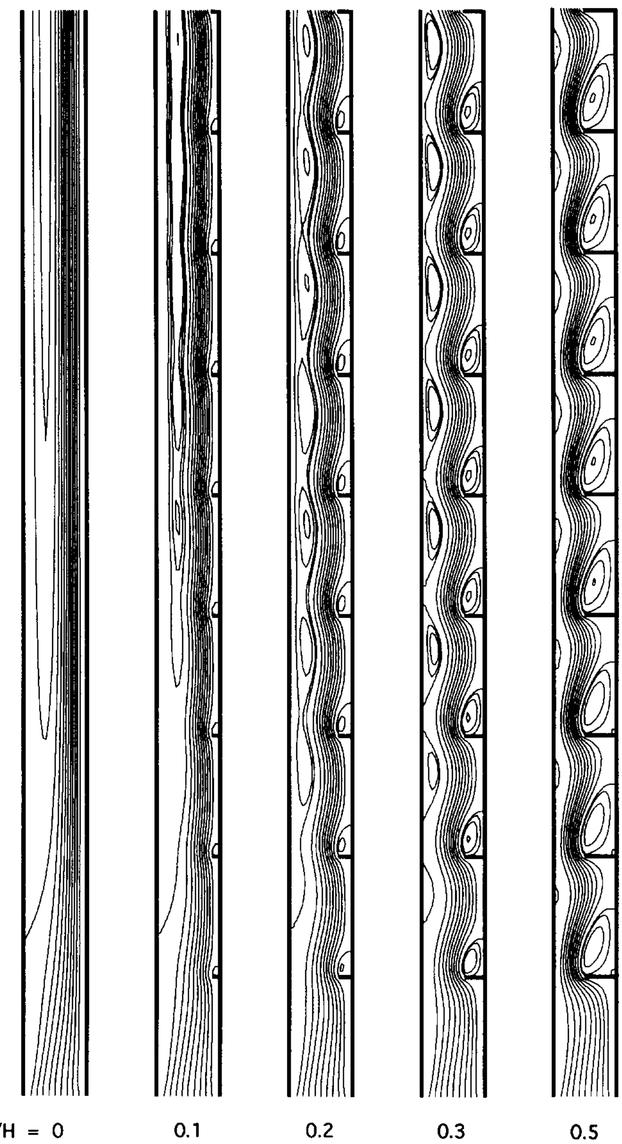

Figure 3 Effect of fin height on flow pattern, for $d/H = 2$, $Gr = 10^5$, and $Re = 100$

recirculation bubbles. The bubbles, one in each module, grow up in size and strength along the axial direction and then become the periodic secondary vortices found by Cheng et al. (1992). The corresponding temperature fields are also shown in Figure 4 to illustrate the development of the thermal boundary layer.

The reason for the occurrence of the flow separation and the recirculation bubbles in Figure 3 may be attributed to an adverse axial pressure gradient developed in the channel, which opposes the inertia and buoyancy forces and supports the occurrence of reversed flow. This adverse pressure gradient will be discussed in the subsequent section.

Table 1 Entrance length of pure forced-convection flow in smooth channels

	x_{FD}/H				
Re	Present study	Brandt and Gillis (1966)	Morihara and Cheng (1973)	Chen (1973)	Narang and Krishnamoorthy (1976)
2	0.639	—	0.651	0.815	0.641
40	1.132	1.130	1.116	1.500	1.110
100	2.446	—	—	2.910	2.725
200	4.694	—	—	—	4.495
400	9.152	9.115	9.030	—	8.350

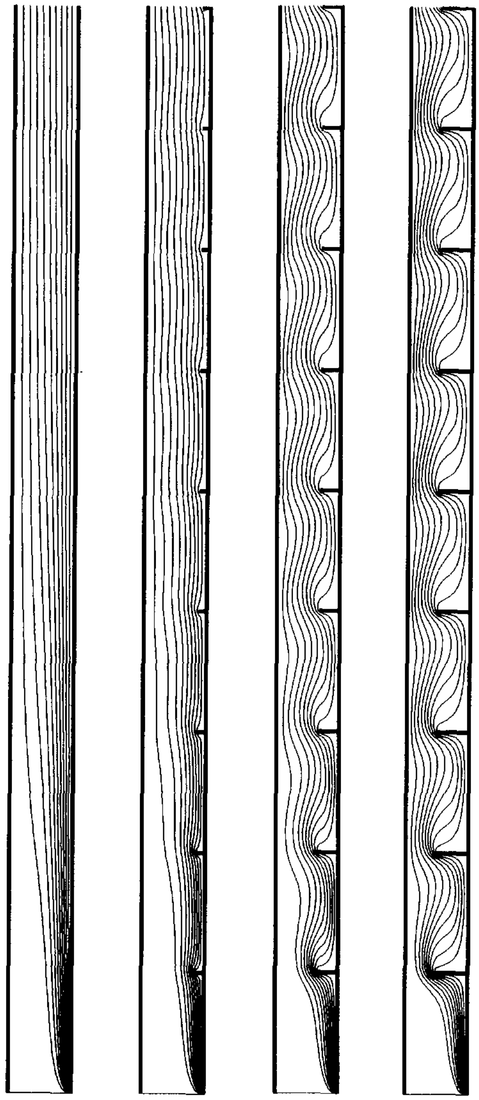

Figure 4 Effect of fin height on temperature distribution, for $d/H = 2$, $Gr = 10^5$, and $Re = 100$

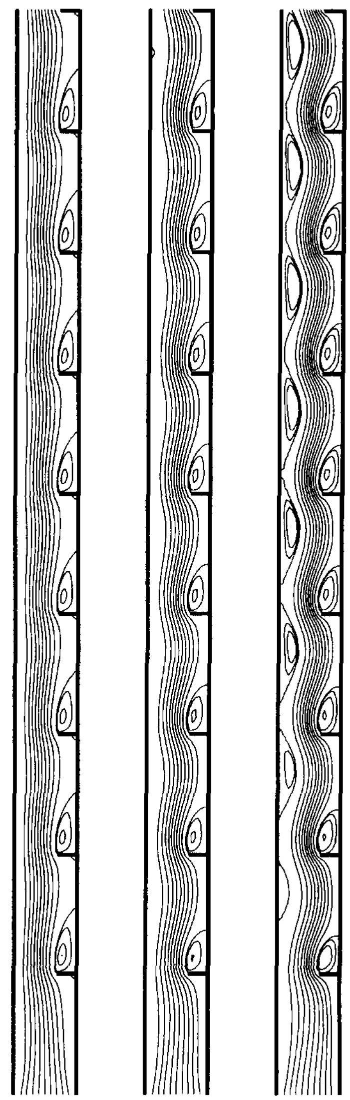

Figure 5 Effect of Grashof number on flow pattern, for $e/H = 0.3$, $d/H = 2$, and $Re = 100$

The buoyancy effect on the flow pattern is shown in Figure 5. For the case of $d/H = 2$, $e/H = 0.3$, and $Re = 100$, a remarkable change in flow pattern caused by the increase of the Grashof number can be observed. It is noticed that as the ratio Gr/Re^2 is raised up to 5, the recirculation bubbles appear and start to grow right after the ninth module. The bubbles become stronger and appear earlier as Gr/Re^2 is increased to 10.

For $e/H = 0.3$, $Re = 100$, and $Gr = 5 \times 10^4$, the influence of pitch length (d/H) on the flow is illustrated in Figure 6. It is found that a larger fin pitch is more encouraging to the reversed flow or recirculation bubble.

To illustrate the development of velocity and temperature fields, Table 2 displays the values of minimum stream function (S_{min}), overall heat transfer (Q_1 and Q_2), and overall pressure gradient (dP/dX) within each module for $e/H = 0.3$, $d/H = 2$, $Re = 100$, and $Gr = 5 \times 10^4$ and 10^5. The fully developed solution of Cheng et al. (1992) is also provided in this table for comparison. It is found that the analytical solution can precisely portray the behavior of developing flow far downstream.

Heat transfer and pressure variation

Attention is drawn to the heat transfer characteristics and pressure variation within the channel. The effect of fin height on pressure variation is illustrated in Figure 7, for $d/H = 2$, $Re = 100$, and $Gr = 5 \times 10^4$. It is observed that the lower-fin case has the larger adverse pressure gradient. This feature basically coincides with that found in Figure 3, which shows that a stronger recirculation bubble will take place in a lower-fin situation.

For the case of $e/H = 0$, Figure 8 shows the pressure variation data for $Re = 100$. The analytical solution of the fully developed pressure gradient given by Cheng et al. (1992) is indicated in this figure for comparison. The excellent agreement is also seen.

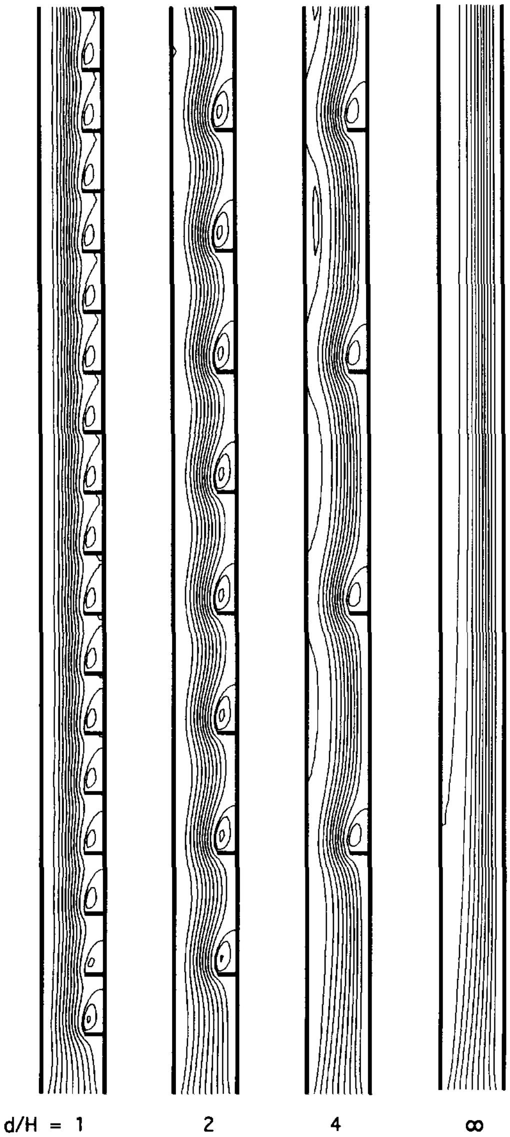

Figure 6 Effect of fin pitch on flow pattern, for $e/H = 0.3$, $Gr = 5 \times 10^4$, and $Re = 100$

The prediction of the influence of fin height on dimensionless local heat fluxes on walls 1 and 2, for $d/H = 2$, $Re = 100$, and $Gr = 10^5$ is shown in Figure 9. It is obvious that heat transfer increases significantly with e/H, since higher fins are employed to provide more heat transfer areas. A periodically varying character of local heat transfer is also found once the fully developed region is reached.

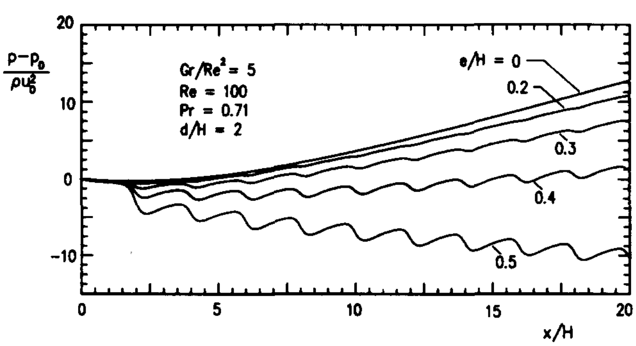

Figure 7 Effect of fin height on streamwise pressure variation, for $d/H = 2$, $Re = 100$, and $Gr = 5 \times 10^4$

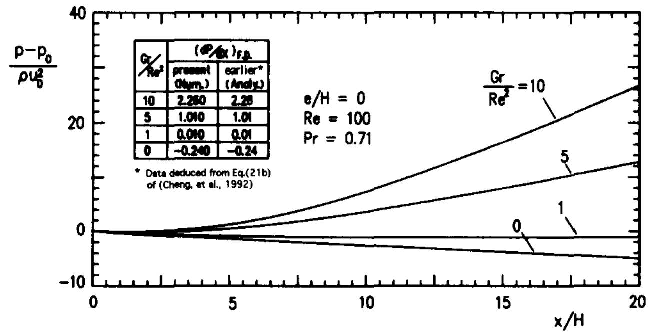

Figure 8 Effect of Grashof number on streamwise pressure variation in a smooth channel, for $Re = 100$

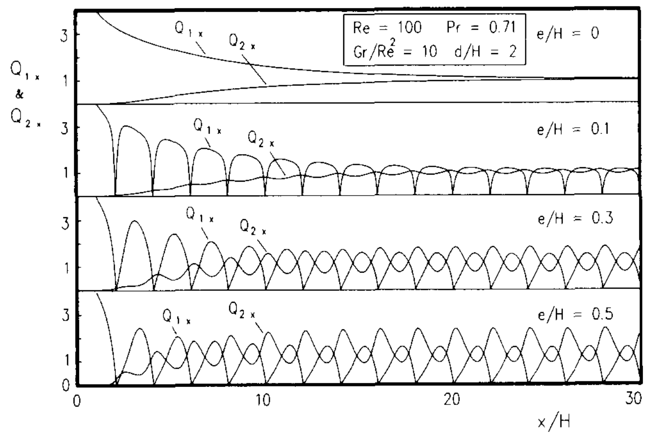

Figure 9 Dependence of local heat fluxes on fin height, for $d/H = 2$, $Re = 100$, and $Gr = 10^5$

Figure 10 shows the variation of heat transfer with fin pitch for $e/H = 0.3$, $Gr = 5 \times 10^4$, and $Re = 100$. The heat transfer characteristic exhibits a rather different feature as d/H is increased.

The overall heat transfer (Q) in the periodically fully developed flow region can be calculated by summation of respective heat transfers from the fin surfaces and the attached wall (wall 1). Table 3 provides the predicted results of overall heat transfer, in terms of Q/Q_0, as a function of d/H, e/H, and Re for the pure forced-convection flow, where the subscript "0" refers to the pure forced-convection flow in a smooth channel. The increase in Q/Q_0 with fin height and Reynolds number is also observed in this table.

For the mixed-convection flow, the effect of buoyancy force (Gr) on overall heat transfer (Q/Q_0) and overall pressure

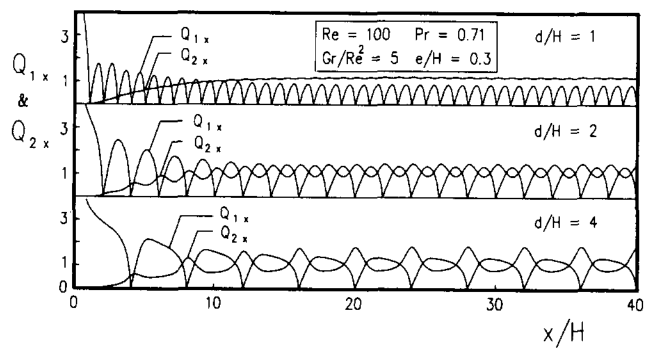

Figure 10 Dependence of local heat fluxes on fin pitch, for $e/H = 0.3$, $Re = 100$, and $Gr = 5 \times 10^4$

Table 2 Streamwise variation of S_{min}, Q_1, Q_2, and dP/dX in each module, for $e/H = 0.3$, $d/H = 2$, Re = 100, and Gr = 5×10^4 and 10^5

	$Gr/Re^2 = 5$				$Gr/Re^2 = 10$			
Module	S_{min}	Q_1	Q_2	dP/dX	S_{min}	Q_1	Q_2	dP/dX
1	0.00000	8.339	0.027	−0.469	0.00000	9.093	0.022	−0.317
2	−0.05243	3.356	0.515	0.033	−0.06426	3.992	0.491	0.408
3	−0.05605	2.750	1.189	0.274	−0.07506	3.154	1.242	0.950
4	−0.05636	2.394	1.624	0.411	−0.07629	2.685	1.736	1.266
5	−0.05661	2.171	1.892	0.495	−0.07691	2.403	2.031	1.449
6	−0.05680	2.031	2.060	0.549	−0.07739	2.228	2.215	1.563
7	−0.05692	1.942	2.167	0.582	−0.07776	2.120	2.330	1.634
8	−0.05700	1.886	2.234	0.604	−0.07811	2.052	2.402	1.678
9	−0.05706	1.850	2.278	0.617	−0.07833	2.010	2.448	1.706
10	−0.05710	1.827	2.305	0.626	−0.07847	1.983	2.477	1.724
11	−0.05712	1.812	2.323	0.632	−0.07856	1.966	2.495	1.735
12	−0.05714	1.803	2.334	0.635	−0.07861	1.956	2.506	1.742
13	−0.05715	1.797	2.342	0.638	−0.07865	1.949	2.513	1.746
14	−0.05716	1.793	2.346	0.639	−0.07867	1.945	2.518	1.749
15	−0.05716	1.791	2.349	0.640	−0.07868	1.942	2.521	1.751
16	−0.05716	1.789	2.351	0.641	−0.07869	1.941	2.522	1.752
17	−0.05716	1.788	2.352	0.641	−0.07870	1.940	2.524	1.752
18	−0.05717	1.787	2.353	0.641	−0.07870	1.939	2.524	1.753
F.D.*	−0.05680	—	2.335	0.648	−0.08198	—	2.497	1.752

* Data presented by Cheng, Luy, and Huang (1992).

Table 3 Q/Q_0 as a function of d/H, e/H, and Re for periodically fully developed forced-convection flow

		Q/Q_0			
d/H	e/H	Re = 50	100	200	300
	0.0	1.000	1.000	1.000	1.000
1	0.1	1.023	1.024	1.025	1.026
	0.3	1.153	1.165	1.187	1.206
	0.5	1.481	1.550	1.635	1.683
	0.0	1.000	1.000	1.000	1.000
2	0.1	1.004	1.004	1.005	1.006
	0.3	1.090	1.106	1.127	1.141
	0.5	1.317	1.384	1.492	1.560
	0.0	1.000	1.000	1.000	1.000
4	0.1	1.009	1.010	1.012	1.013
	0.3	1.051	1.070	1.100	1.125
	0.5	1.187	1.273	1.360	1.401

gradient $((dP/dX)/(dP/dX)_0)$ of periodically fully developed flow is shown in Table 4. For $d/H = 2$ and $e/H = 0.3$, it is found that the buoyancy force will improve the heat transfer significantly and produce an adverse pressure gradient in the channel, an effect that has already been observed in Figures 7 and 8.

It is important to mention here that four gridpoint systems, namely, 801 × 21, 1201 × 31, 1601 × 41, and 2001 × 51, are tested to ensure the grid independence of the numerical solutions. Table 5 shows the results of S_{min} within each module obtained from various grid systems for a typical case $e/H = 0.3$, $d/H = 2$, Re = 100, and Gr = 5×10^4 and 10^5. It is found that for almost all cases considered in this study, the relative error in the comparison of solutions between 1601 × 41 and 2001 × 51 is within 1 percent; however, the increase in computer effort for 2001 × 51 is considerable.

Concluding remarks

Numerical prediction of the buoyancy effect on the developing flow in a vertical channel with fin array has been performed.

Table 4 Effect of Gr on Q/Q_0 and $(dP/dX)/(dP/dX)_0$ for periodically fully developed flow with $d/H = 2$, $e/H = 0.3$

	Q/Q_0				$(dP/dX)/(dP/dX)_0$			
Gr	Re = 50	100	200	300	Re = 50	100	200	300
10^3	1.103	1.118	1.139	1.153	1.557	1.886	2.171	2.288
5×10^3	1.107	1.122	1.141	1.154	0.783	1.513	1.994	2.170
10^4	1.113	1.126	1.143	1.155	−0.187	1.042	1.770	2.023
5×10^4	1.205	1.167	1.163	1.167	−7.899	−2.705	−0.019	0.839
10^5	1.395	1.249	1.190	1.182	−17.092	−7.300	−2.262	−0.634

Table 5 Grid independence check, for $e/H = 0.3$, $d/H = 2$, and Re = 100

	S_{min}							
	$Gr/Re^2 = 5$				$Gr/Re^2 = 10$			
Module	2001 × 51	1601 × 41	1201 × 31	801 × 21	2001 × 51	1601 × 41	1201 × 31	801 × 21
1	0.00000	0.00000	0.00000	0.00000	0.00000	0.00000	0.00000	0.00000
2	−0.05235	−0.05243	−0.05579	−0.06003	−0.06503	−0.06426	−0.06098	−0.05861
3	−0.05589	−0.05605	−0.05907	−0.06264	−0.07689	−0.07506	−0.06961	−0.06694
4	−0.05619	−0.05636	−0.05933	−0.06301	−0.07710	−0.07629	−0.07083	−0.06809
5	−0.05643	−0.05661	−0.05987	−0.06355	−0.07776	−0.07691	−0.07144	−0.06873
10	−0.05692	−0.05710	−0.06035	−0.06420	−0.08013	−0.07847	−0.07301	−0.07001
30	−0.05700	−0.05717	−0.06043	−0.06431	−0.08050	−0.07871	−0.07336	−0.07025
40	−0.05700	−0.05717	−0.06044	−0.06431	−0.08050	−0.07871	−0.07336	−0.07025

The results of various physical parameters are presented to show their influence on flow pattern and thermal characteristics. In general, when hotter-wall heating is sufficiently strong, an adverse pressure gradient may develop within the channel, and then a series of buoyancy-induced recirculation bubbles may appear, one in each module, near the colder wall. These bubbles increase in size and strength along the axial direction and then turn to the periodically fully developed secondary vortices found by Cheng et al. (1992). For the limiting case of $e/H = 0$ (smooth channel), these bubble areas become a continuous zone of reversed flow, which has been relatively well analyzed by Aung and Worku (1986a, 1986b) and Cheng et al. (1990).

On the other hand, heat transfer increases significantly with fin height (e/H) due to the additional heat transfer areas. Meanwhile, the buoyancy effect can also improve the heat transfer performance.

The results of this study have been compared with some existing benchmark solutions to ensure the validity of the numerical methods. All these comparisons exhibit satisfactory accuracy of the present numerical solutions.

References

Aung, W. and Worku, G. 1986a. Developing flow and flow reversal in a vertical channel with asymmetric wall temperatures. *J. Heat Transfer*, **108**, 299–304

Aung, W. and Worku, G. 1986b. Theory of fully developed, combined convection including flow reversal. *J. Heat Transfer*, **108**, 485–488

Berner, C., Durst, F., and McEligot, D. M. 1984. Flow around baffles. *J. Heat Transfer*, **106**, 743–749

Brandt, A. and Gillis, J. 1966. Magnetohydrodynamic flow in the inlet region of a straight channel. *Phys. Fluids*, **9**, 690–699

Chen, R. Y. 1973. Flow in entrance region at low Reynolds numbers. *J. Fluids Eng.*, **9**, 153–158

Cheng, C. H. and Huang, W. H. 1989. Laminar forced convection flows in horizontal channels with transverse fins placed in entrance regions. *Numer. Heat Transfer*, **16**, 77–100

Cheng, C. H., Kou, H. S., and Huang, W. H. 1990. Flow reversal and heat transfer of fully developed mixed convection in vertical channels. *J. Thermophys. Heat Transfer*, **4**, 375–383

Cheng, C. H. and Huang, W. H. 1991. Numerical prediction for laminar forced convection in parallel-plate channels with transverse fin arrays. *Int. J. Heat Mass Transfer*, **34**, 2739–2749

Cheng, C. H., Luy, C. D., and Huang, W. H. 1992. Buoyancy effect on the heat transfer in vertical channels with fin arrays at low Reynolds numbers. *Int. J. Heat Mass Transfer*, **35**, 2643–2653

Durst, F., Founti, M., and Obi, S. 1988. Experimental and computational investigation of the two-dimensional channel flow over two fences in tandem. *J. Fluids Eng.*, **110**, 48–54

Kelkar, K. M. and Patankar, S. V. 1987. Numerical prediction of flow and heat transfer in a parallel plate channel with staggered fins. *J. Heat Transfer*, **109**, 25–30

Lazaridis, A. 1988. Heat transfer correlation for flow in a parallel-plate channel with staggered fins. *J. Heat Transfer*, **110**, 801–802

Luy, C. D., Cheng, C. H., and Huang, W. H., 1991. Forced convection in parallel-plate channels with a series of fins mounted on the wall. *Appl. Energy*, **39**, 127–144

Morihara, H. and Cheng, R. T. 1973. Numerical solution of viscous flow in the entrance region of parallel plates. *J. Computational Phys.*, **11**, 500–572

Narang, B. S. and Krishnamoorthy, G. 1976. Laminar flow in the entrance region of parallel plates. *J. App. Mech.*, **43**, 186–188

Patankar, S. V., Liu, C. H., and Sparrow, E. M. 1977. Fully developed flow and heat transfer in ducts having streamwise-periodic variation of cross-sectional area. *J. Heat Transfer*, **99**, 180–186

Shah, R. K. and London, A. L. 1978. Laminar flow forced convection in ducts. In *Advances in Heat Transfer*, Suppl. 1, T. F. Irvine and J. P. Hartnett (eds.), Academic Press, New York

Sparrow, E. M., Baliga, B. R., and Patankar, S. V. 1978. Forced convection heat transfer from a shrouded fin array with and without tip clearance. *J. Heat Transfer*, **100**, 572–579

Webb, B. W. and Ramadhyani, S. 1985. Conjugate heat transfer in a channel with staggered ribs. *Int. J. Heat Mass Transfer*, **28**, 1679–1687